Journal of Medicinal Chemistry

Article

Discovery of 2-Pyridinone Aminals: A Prodrug Strategy to Advance a Second Generation of HIV-1 Integrase Strand Transfer Inhibitors

Izzat Raheem, Abbas Walji, Daniel Klein, John M. Sanders, David Powell, Pravien Abeywickrema, Guillaume Barbe, Amrith Bennet, Sophie-Dorothee Clas, David Dubost, Mark Embrey, Jay Grobler, Michael Hafey, Timothy John Hartingh, Daria J. Hazuda, Michael D. Miller, Keith P. Moore, Natasa Pajkovic, Sangita Patel, Vanessa Rada, Paul Rearden, John D. Schreier, John Sisko, Thomas G. Steele, Jean-François Truchon, John Wai, Min Xu, and Paul J Coleman

J. Med. Chem., **Just Accepted Manuscript** • DOI: 10.1021/acs.jmedchem.5b01037 • Publication Date (Web): 23 Sep 2015

Discovery of 2-Pyridinone Aminals: A Prodrug Strategy to Advance a Second Generation of HIV-1 Integrase Strand Transfer Inhibitors

Izzat T. Raheem‡[a], Abbas M. Walji*‡[a], Daniel Klein[b], John M. Sanders[b], David A. Powell[a,i], Pravien Abeywickrema[c], Guillaume Barbe[i], Amrith Bennet[d], Sophie–Dorothee Clas[j], David Dubost[e], Mark Embrey[a], Jay Grobler[f], Michael J. Hafey[g], Timothy J. Hartingh[a], Daria J. Hazuda[f], Michael D. Miller[f], Keith P. Moore,[a] Natasa Pajkovic[g], Sangita Patel,[b] Vanessa Rada[a], Paul Rearden[g], John D. Schreier[a], John Sisko[a], Thomas G. Steele[a], Jean–François Truchon[i], John Wai[a], Min Xu[h], and Paul J. Coleman[a].*

Departments of Discovery Chemistry[a], Global Structural Chemistry[b], Protein Sciences[c], Safety Assessment[d], Discovery Pharmaceutical Sciences[e], Infectious Disease Biology[f], Pharmacokinetics, Pharmacodynamics, and Drug Metabolism[g], and In Vitro Pharmacology[h] Merck Research Laboratories, West Point, PA 19486.

Merck Frosst Centre for Therapeutic Research[i], Kirkland, QC, Canada.

PharmaSolv Consulting[j], Montreal, QC, Canada.

ABSTRACT

The search for new molecular constructs that resemble the critical 2-metal binding pharmacophore required for HIV integrase strand transfer inhibition represents a vibrant area of research within drug discovery. Here we present the discovery of a new class of HIV integrase strand transfer inhibitors based on the 2-pyridinone core of MK-0536. These efforts led to the identification of two lead compounds with excellent antiviral activity and preclinical pharmacokinetic profiles to support a once-daily human dose prediction. Dose escalating PK studies in dog revealed significant issues with limited oral absorption and required an innovative prodrug strategy to enhance the high-dose plasma exposures of the parent molecules.

INTRODUCTION

Over the past 20 years, Merck & Co. Inc. has made a strong commitment towards identifying new antiretroviral (ARV) treatments to help patients infected with the HIV-1 virus. To this end, we validated strand transfer (ST) inhibition as a new therapy, and in 2007 successfully launched raltegravir (**1**, RAL) as the first HIV-1 integrase strand transfer inhibitor (InSTi).[1-3] RAL has established robust efficacy and tolerability in treatment-naïve patients and is considered a preferred first-line ARV agent as part of highly active antiretroviral therapy (HAART).[4]

The success of RAL represents an important addition to the armamentarium of ARV agents and has sparked significant interest in developing the next generation of HIV InSTis. The main challenges in enhancing efficacy and patient compliance are associated with reducing the dosing frequency to once daily, and improving the genetic barrier to resistance.[5] As a result there has been a surge of research activity to address these limitations with significant contributions from both academia and industry.[4,6,7] The main focus has been on the identification of new chemical

classes able to retain the intrinsic potency and structural elements of a bidentate metal-binding pharmacophore, which is essential for strand transfer inhibition. These efforts have provided several distinct structural classes and resulted in the notable discoveries of elvitegravir (**2**, ELV)[8,9] from Gilead Sciences, dolutegravir (**3**, DTG)[10] developed by a Shionogi-ViiV Healthcare-GlaxoSmithKline joint venture, and MK-2048 (**4**)[11,12] and MK-0536 (**5**)[13,14] from Merck & Co. Inc (Scheme 1).

Scheme 1. Current leading HIV integrase strand transfer inhibitors: two-metal binding pharmacophore highlighted in blue.

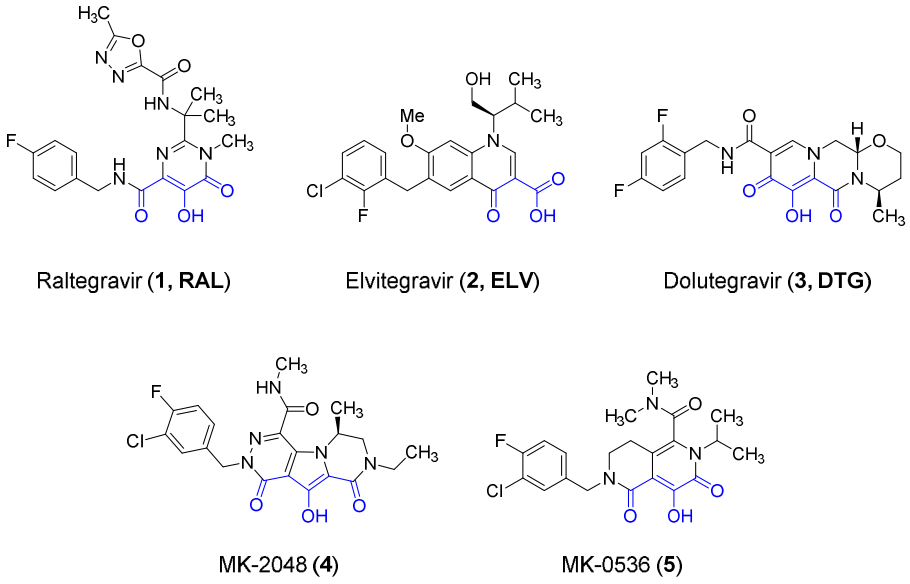

ELV (**2**), approved in 2012, has a reduced dosing frequency to once-daily (150 mg) when co-dosed with a cytochrome P450 inhibitor, but confers significant cross resistance to RAL. DTG (**3**), approved in 2013, has differentiated potency against viral clones resistant to RAL and ELV, and does not require pharmacokinetic boosting to enable once-daily dosing. MK-2048 and MK-0536 provide a similar superior barrier to resistance as DTG, with MK-2048 exhibiting potential

as a microbicide for prevention of HIV infection.[12b] MK-0536 represents a new structural class based on the 2-pyridinone core which is currently under investigation in our laboratories.

We have previously disclosed our lead finding and lead optimization efforts culminating in the identification of MK-0536.[14] MK-0536 exhibits excellent antiviral activity as measured in a viral kinetics assay (IP 50% NHS = 53 nM) and also retains activity against RAL-resistant mutants with a maximum 3-fold shift against N155H (Table 1). This robust activity against a wide range of integrase variants suggests that MK-0536 has the potential for a high genetic barrier for the development of resistance. Furthermore, it displays a reasonable preclinical pharmacokinetic (PK) profile in rat (CL_p = 2.3 mL/min/kg, %F = 29) and dog (CL_p = 2.2 mL/min/kg, %F = 44), and low intrinsic clearance (CL_{int}) in vitro in human hepatocytes (CL_{int} = <20 mL/min/kg). Using single-species allometric scaling of dog plasma clearance and correcting for the difference in plasma protein binding between the species, the human plasma clearance was predicted to be approximately 1 mL/min/kg.[15]

Table 1. Inhibitory potency and mutation profiles of RAL and MK-0536.

		Fold shift of IP in potency assay[a] for mutant virus vs. wild-type (WT) virus (50% NHS)				
Compound	WT IP[b]	E92Q	Y143R	Q148R	Q148K	N155H
RAL	9 / 53 nM	3	13	16	22	8
MK-0536	6 / 53 nM	1	2	1	1	3

[a] kinetic HIV replication assay[16] [b] IP in 0 / 50% NHS.

During our discovery efforts towards MK-0536, we identified several structural modifications within the 2-pyridinone scaffold which provided new opportunities for lead optimization.

Herein, we describe the discovery of two lead molecules from within a novel tricyclic 2-pyridinone aminal series. In an effort to advance these molecules into preclinical safety studies, we implemented an innovative prodrug strategy to overcome absorption-limiting physicochemical properties and achieve our targeted plasma exposures of the parent compounds.

RESULTS AND DISCUSSION

A deeper understanding of HIV-1 integrase inhibition and resistance as well as the use of structure-guided design of small molecule HIV-1 integrase inhibitors has been hampered by the inability to crystallize a ligand-bound HIV-1 integrase intasome. However, the structure of the related prototype foamy virus (PFV) intasome was recently solved.[17] While PFV integrase and HIV integrase share less than 20% sequence identity, there is a high degree of sequence conservation in their active sites. As such, it is currently believed that PFV integrase structures serve as reliable models of the HIV integrase active site, and could facilitate structure-guided small molecule inhibitor design. To date, numerous structures of HIV integrase inhibitors bound to the PFV integrase intasome have been reported.[18]

Using MK-0536 as a starting point, and guided in part by computational docking of MK-0536 in the PFV integrase active site, we sought to explore structural diversity of the 2-pyridinone core through fusion of a third ring. Our docked structure of MK-0536 (Figure 1), together with the crystal structure of RAL, supported the hypothesis that a ring fusion in the northeastern portion of the 2-pyridinone core would be tolerated by HIV integrase. Additionally, we hoped to maintain the beneficial PK attributes and optimal mutation profile imparted by the MK-0536 bicyclic framework in these elaborated inhibitors. Over the course of our lead optimization

efforts, numerous such cyclization strategies were explored, a subset of which are shown in Figure 2.

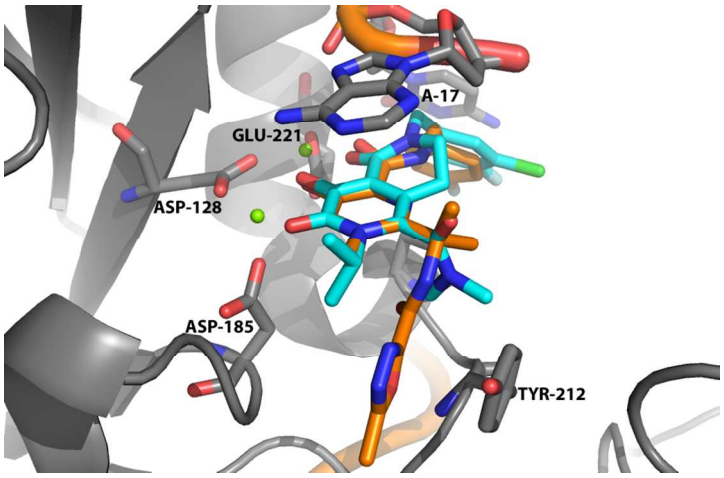

Figure 1. Overlay of modeled MK-0536 (cyan) and crystallographic RAL (orange) in the catalytic active site of PFV Integrase (PDB 3oya).

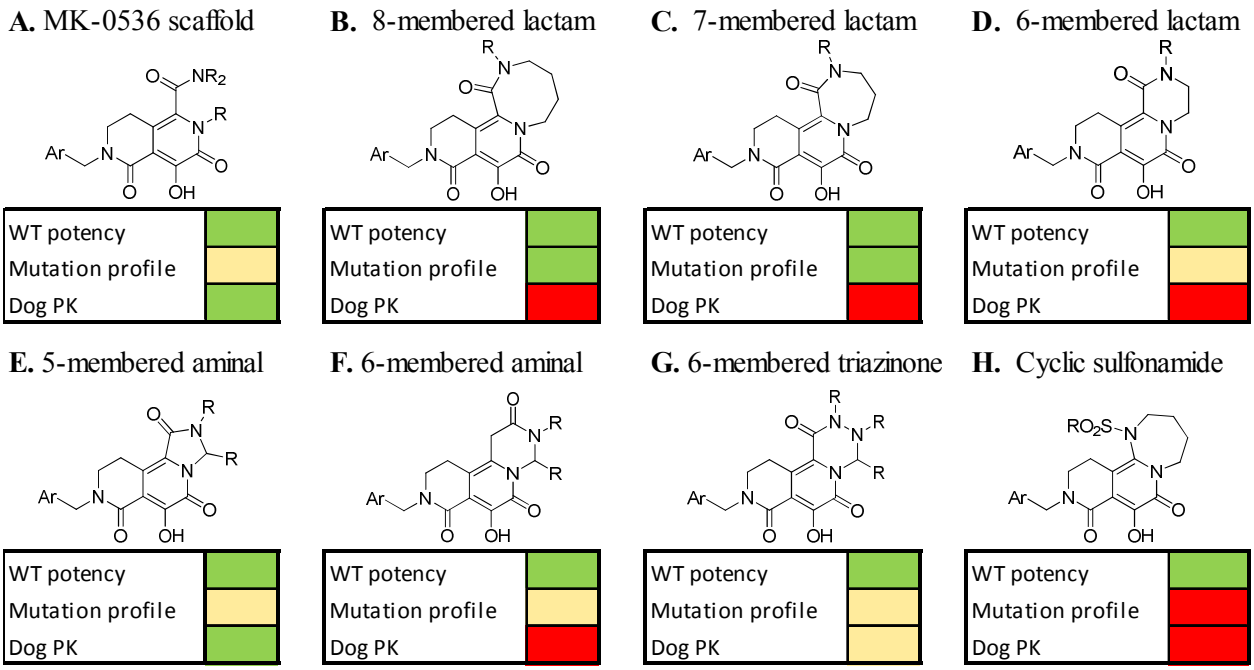

Figure 2. Overview of C-ring cyclization strategies and general scaffold profiles. General approximations for profile rankings of scaffolds – WT Potency (IP in 10% NHS): Green= <100 nM, Yellow= 100–250 nM, Red= >250 nM; Mutation profile (IP shift vs. least sensitive

mutant): Green= <5 fold shift, Yellow= 5–15 fold shift, Red= >15 fold shift; Dog PK (CL_p): Green= <10 mL/min/kg, Yellow= 10–20 mL/min/kg, Red= >20 mL/min/kg.

Due in part to more facile synthetic access, we initially targeted a series of variably-sized amido-containing ring systems. The 8- and 7-membered ring systems (Figure 2B and 2C) provided inhibitors that generally displayed excellent WT potencies and resistance profiles, but suffered from high unbound clearances (CL_{un}) in dog. The corresponding 6-membered ring system (Figure 2D) provided potent inhibitors with compromised mutation and PK profiles. We were gratified to discover that the fused 5-membered ring system (Figure 2E) provided an optimal balance between potency and PK. In general, inhibitors in this structural class were extremely potent on the wild-type enzyme as measured in the viral kinetics assay[16] (IP 0% NHS < 10 nM), with promising mutation profiles. Importantly, they displayed low CL_p and CL_{un} in preclinical species, akin to MK-0536. Additionally, despite the presence of an aminal-type functionality, compounds were chemically and configurationally stable upon isolation.

Two distinct homologation strategies of this promising ring system were further investigated: (a) homologation by one carbon gave the corresponding 2-pyridinone 6-membered ring scaffolds (Figure 2F) and (b) homologation by one nitrogen (Figure 2G) afforded the corresponding triazinone 2-pyridinone. While compounds in these 6-membered ring classes exhibited good-to-moderate mutation profiles, PK properties were typically compromised. Numerous other non-amido tricyclic cores were also interrogated. One specific example is the dihydroimidazole ring system highlighted in Figure 2H. This core, like many others interrogated, provided inhibitors with poor mutation and PK profiles.

Based on this analysis the 5-membered aminal ring system was selected for further exploration. Through an extensive lead optimization effort, key points of diversity around the

periphery of the 2-pyridinone aminal framework were thoroughly interrogated; an SAR overview is presented in Figure 3. A western aromatic group (R_1) is present in nearly all published HIV-1 InSTis, and serves as a crucial hydrophobic π-clamp in the catalytic active site. Historically, a halogenated benzyl moiety in this position has been optimal, and the same was found to be true for the 2-pyridinone aminals. While some R_1 variations were identified that allowed for modulation of compound physical properties, little structural variation was tolerated, with all compounds of interest bearing a 4-fluoro-3-chlorobenzyl or 4-fluorobenzyl group.

While substituent changes at the R_2/R_3 position did not significantly impact WT potency, they did provide us the opportunity to modulate other important properties of our compounds. The SAR at R_2/R_3 proved to be extremely narrow, with only a select number of small cyclic aliphatic groups providing acceptable resistance profiles against key single mutants.

Finlly, the R_4 position was found to be most tolerant of structural variation, facilitating optimization of potency, resistance profile, physical properties, and PK parameters. The position tolerated diversity in size, polarity, functional group, and H-bond donor/acceptor capacity, allowing us to prepare and characterize a number of distinct leads.

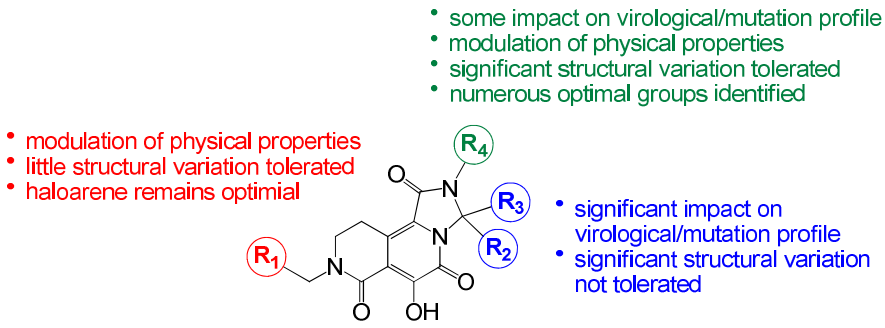

Figure 3. Overview of 2-pyridinone aminal series SAR

Our optimization efforts led initially to **6** (Table 2), an important benchmark compound for the series. Its key structural feature is a novel bicyclo[3.1.0]hexane ring system at the R_2/R_3 aminal position; the R_1 position maintains the aforementioned 4-fluoro-3-chlorobenzyl group and R_4 is unsubstituted. Beyond its structural novelty, **6** exhibits excellent intrinsic antiviral activity (WT IP 0% NHS = 2.5 nM), but a large shift in serum potency attributed to high plasma protein binding (WT IP 50% NHS = 600 nM). **6** displays a good resistance profile against RAL-resistant mutants with a maximum 6-fold shift against Q148K. Additionally, it displays low clearance and moderate oral bioavailability in rat (CL_p = 0.12 mL/min/kg, %F = 29) and dog (CL_p = 0.15 mL/min/kg, %F = 27), and low Cl_{int} in vitro in human hepatocytes (CL_{int} = <5 mL/min/kg).

Table 2. Inhibitory potency, mutation profile, and pharmacokinetic profile of **6**.

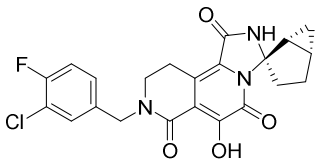

	Fold shift of IP in potency assay[a] for mutant virus vs. wild-type (WT) virus (50% NHS)				
WT IP[b]	E92Q	Y143R	Q148R	Q148K	N155H
2.5 / 600 nM	3	1	5	6	3

	Intravenous			Oral	
species (IV / PO dose)	Cl_p (mL/min/kg)	V_{dss} (L/kg)	$T_{1/2}$ (hr)	AUC $(\mu M \cdot hr)_{0\text{-}inf}$	F (%)
rat (0.2 / 2 mg/kg)	0.12	0.12	14	189	29
dog (0.5 / 2 mg/kg)	0.15	0.19	16	47	27

[a] kinetic HIV replication assay[16] [b] IP in 0 / 50% NHS.

Based on the above SAR analysis of the 2-pyridinone aminal core and the promising profile of **6**, further optimization efforts were undertaken employing divergent functionalization strategies starting from compound **6** (Scheme 2). The objective was to improve the serum-shifted potency by increasing the polar surface area (PSA) at the predefined R_2/R_3 and R_4 positions. For compounds within this series, we identified the introduction of free hydroxyl groups as optimal polarity-enhancing groups, providing the necessary balance among potency, mutation profile, and preclinical PK profile. These efforts yielded two lead molecules: compound **7** bearing a chiral secondary alcohol on the alkyl chain of the aminal nitrogen (R_4 optimization), and compound **8** incorporating a hydroxymethyl substituent (R_2/R_3 optimization) at the optimal position on the bicyclo[3.1.0]hexane ring system.

Scheme 2. Lead optimization starting from compound **6**: strategic introduction of free alcohols at R_2/R_3 and R_4 to increase polar surface area.

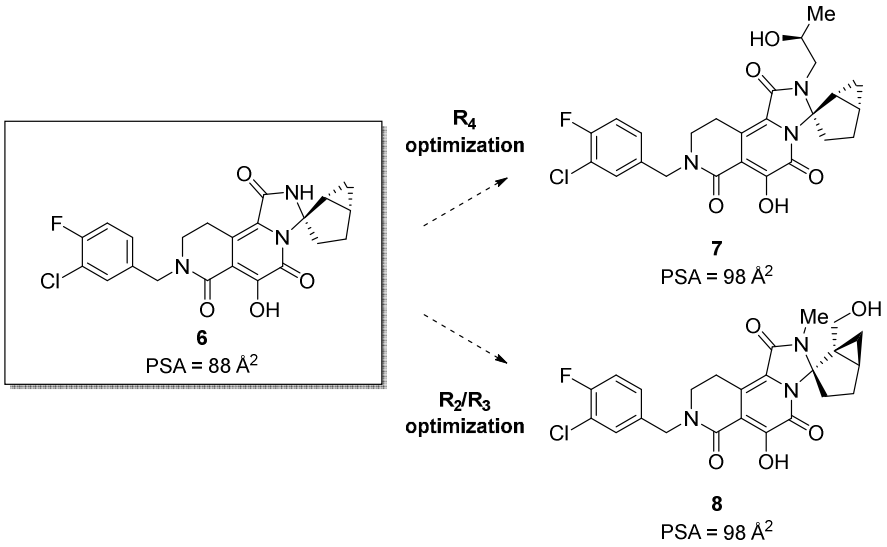

As summarized in Table 3, both compounds maintain excellent potency against the wild-type virus (WT IP 50% NHS <75 nM), and extremely low fold-shifts in potency against RAL-

resistant mutants. Co-crystal structures for compounds **7** and **8** bound to the PFV intasome complex revealed noteworthy interactions previously suggested as important for both potency and the favorable mutation profile required of a second-generation strand transfer inhibitor.[17a] Both **7** and **8** adopt low-energy bioactive conformations, as judged by having relative ΔG values <1 kcal/mol as calculated by the FreeForm program,[19] and are characterized by their direct interactions with two Mg^{2+} ions and burial of the hydrophobic 4-fluoro-3-chlorobenzyl groups between the terminal DNA base pair and Pro214 (Figure 4A). Although of differing stereochemistry, the substituted bicyclo[3.1.0]hexane groups of **7** and **8** each make increased contact with Gly187 in the β4-α2 loop as compared to MK-0536 and other first-generation InSTis and therefore resemble the interactions observed with DTG and MK-2048 (Figure 4B).[17a,18a] In the observed binding conformations, the polarity-enhancing hydroxyl groups of **7** and **8** make no direct interactions with protein or DNA, consistent with the apparent selective impact of these groups on improving potency under high serum concentration conditions. While the protein residues are largely unchanged when compared to other PFV intasome inhibitor complexes, the 3'-terminal unpaired adenosine, A(-17), adopts the less energetically favorable of the two predominant conformations that have been previously observed (Figure 4A).[18b] Taken together, the structural data demonstrate that 2-pyridinone aminals display excellent HIV integrase inhibition even without forming extensive interactions between the tricyclic core and A(-17).

Table 3. Inhibitory potency and mutation profiles of **7** and **8**.

Compound	WT IP[b]	Fold shift of IP in potency assay[a] for mutant virus vs. wild-type (WT) virus (100% NHS)				
		E92Q	Y143R	Q148R	Q148K	N155H
7	2 / 67 nM	1.5	1	1.5	1	1.5
8	3 / 32 nM	1	1	1	1	1

[a] kinetic HIV replication assay[16] [b] IP in 0 / 50% NHS.

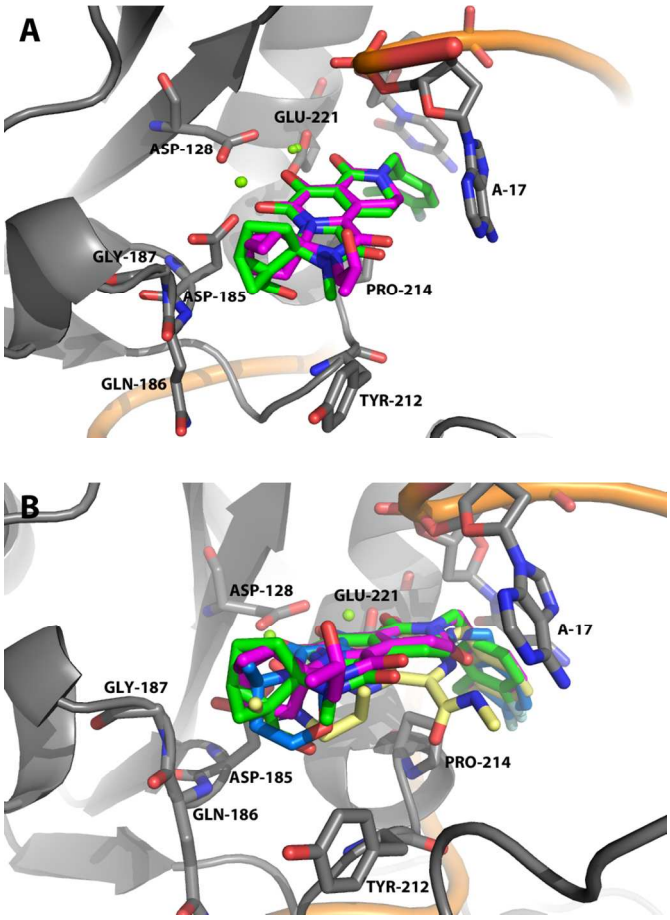

Figure 4. A) Crystal structure overlay of **7** (magenta) and **8** (green) in the PFV catalytic active site. B) Overlay of **7**, **8**, DTG (blue, from PDB 3s3m) and MK-2048 (yellow, from PDB 3oyb), illustrating inhibitor contacts with β4-α2 loop.

Compounds **7** and **8** were tested in intravenous (iv) and oral (p.o.) PK studies in beagle dogs (Tables 4). After iv administration both compounds exhibited low plasma clearance with terminal half-lives ranging from 5–6 h. The oral bioavailabilities for **7** and **8** were 42% and 26% respectively. Plasma protein binding for both compounds was high with measured values of 98.8 and 97.5% in dog and human for compound **7**, and 98.6 and 98% in dog and human for compound **8**. The major route of elimination of these compounds was glucuronidation, while cytochrome P450 (CYP) mediated oxidative metabolism was a minor contributing pathway. The intrinsic clearances in vitro in human hepatocytes ranged from CL_{int} = 14–26 mL/min/kg. The compounds were not potent reversible inhibitors of the major isoforms of the CYP enzymes (3A4, 2C9, or 2D6), nor time-dependent inhibitors of CYP3A4. Both lead compounds exhibited very similar pharmacokinetic properties in preclinical species to those observed with MK-0536, and using the same methods as previously described the human plasma clearance was predicted to be approximately 1 mL/min/kg for both compounds. The steady-state plasma $AUC_{0\text{-}24hr}$ for the predicted human once-daily doses for our leads was between 30 μM•hr and 50 μM•hr.

Table 4. Pharmacokinetic profiles of **7** and **8** in beagle dog**.**

		Intravenous			Oral	
Compound	iv/p.o. dose	Cl_p (mL/min/kg)	V_{dss} (L/kg)	$T_{1/2}$ (hr)	AUC $(\mu M \cdot hr)_{0\text{-}inf}$	F (%)
7	0.5 / 2 mg/kg	3.0	0.6	5.9	10.5	42
8	0.5 / 1 mg/kg	1.9	0.4	5	4.9	26

Chemistry. Lead compounds **7** and **8** are both prepared from tris-pivaloylated 2-pyridinone intermediate **14**. The synthesis of **14** is shown in Scheme 3, and begins with known α,β-unsaturated sulfone **9**.[4] Conjugate addition of ethyl 2-((diphenylmethylene)-amino)acetate followed by imine hydrolysis provides **10**, which is treated with DIPEA to effect elimination to **11**. Condensation with ethyl oxalyl chloride furnishes the full bicyclic 2-pyridinone core **12**, which is then hydrolyzed and tripivaloylated, to afford key intermediate **14**.

Scheme 3. Synthesis of tris-pivaloylated intermediate **14**.

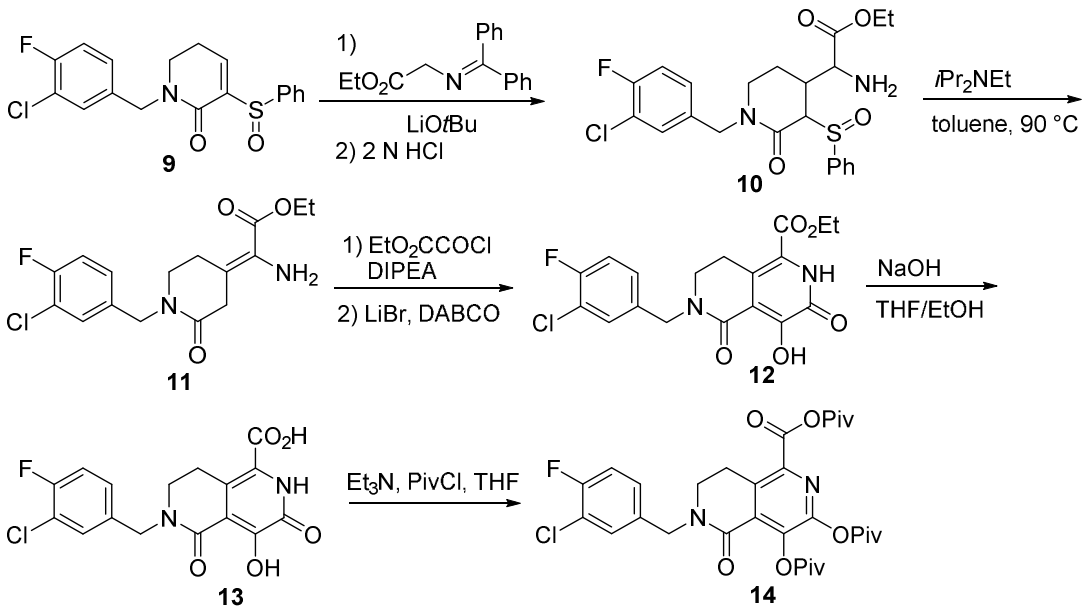

The known chiral ketone building block **18** is synthesized in three steps (Scheme 4). The reaction of (*R*)-epichlorohydrin with allyl magnesium chloride and copper iodide furnishes **16**, which undergoes base-mediated cyclization to provide the bicyclic framework. Oxidation of the secondary alcohol with TPAP/NMO gives ketone **18.**

Scheme 4. Synthesis of chiral ketone building block **18**.[20]

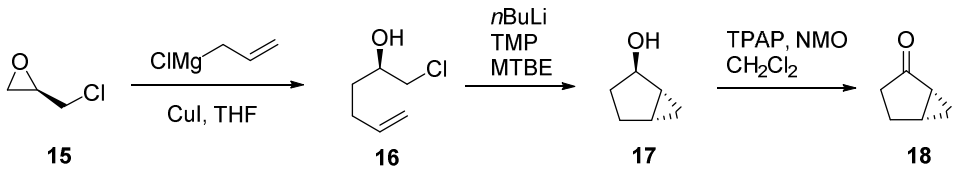

With **14** and **18** in hand, compound **7** is prepared in two steps, as shown in Scheme 5. First, **14** is reacted with commercially available chiral amine **19**. Under these conditions, one of the pivaloyl moieties acylates the primary amine while the other two are hydrolyzed, furnishing **20** in near quantitative yield. Intermediate **20** is then condensed with chiral ketone **18** under forcing conditions to provide the tricyclic 2- pyridinone aminal **7.**

Scheme 5. Synthesis of **7**.

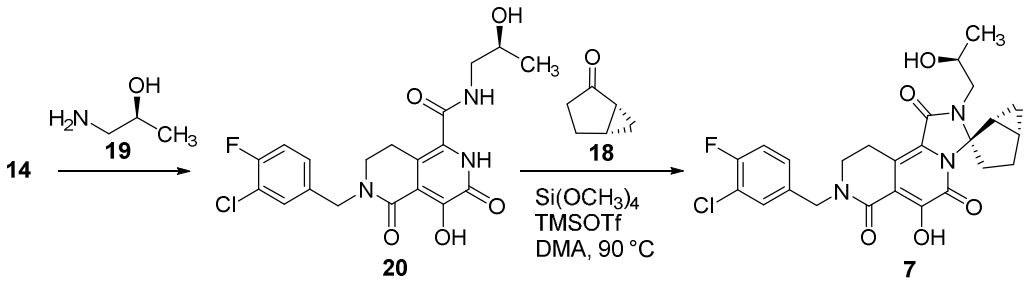

Compound **8** is prepared from intermediate **14** in four steps (Scheme 6). Treatment of **14** with ammonium hydroxide furnishes primary amide **21**, which undergoes condensation with known chiral keto-ester **22**[21] under conditions similar to those described above. The resulting aminal is methylated under standard conditions, and the pendant ester is reduced with $LiBH_4$ to furnish **8**.

Scheme 6. Synthesis of **8**.

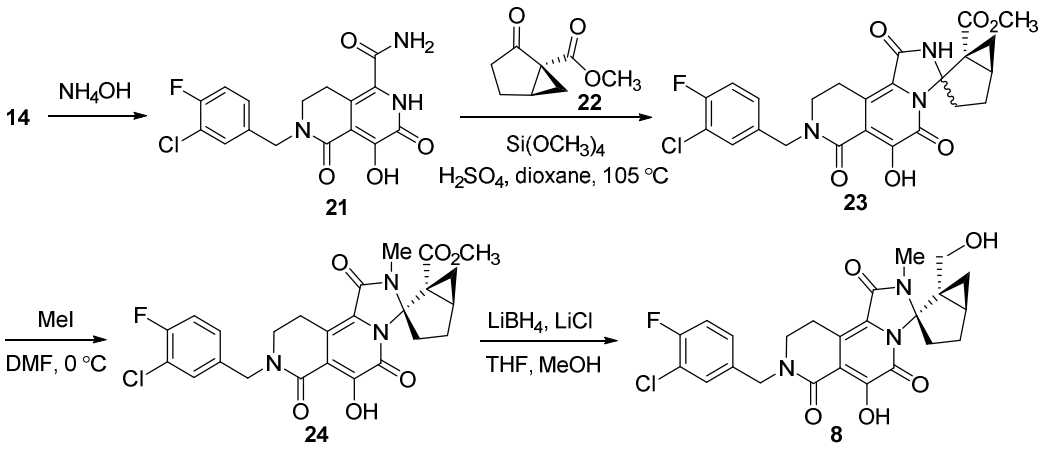

Prodrug Strategy to Address PK Limitations. Our focused lead optimization efforts from compound **6** were successful in discovering two 2nd generation HIV InSTis, which offered potential improvements over known InSTis. First, both compounds exhibited superior barrier to resistance compared to RAL and ELV, and second, they displayed preclinical PK profiles consistent with once-daily human dose predictions without the need for a PK enhancer.

However, we uncovered a significant limitation as we evaluated these compounds in non-rodent (beagle dog) dose escalating oral PK studies. We observed an early plateau in plasma exposure following the first 5-fold increase in dose (2 mg/kg to 10 mg/kg) for both lead compounds (Figure 5); this exposure plateau persisted further as the dose was increased to 30 mg/kg. In light of low plasma clearance and moderate bioavailabilities, we speculated that the less than dose proportional increase in exposure was likely due to poor physicochemical properties for both lead molecules. Indeed, this was verified by low crystalline solubility in fasted simulated intestinal fluid (FaSSiF) and simulated gastric fluid (SGF). Further, in vitro passive permeability in LLC-PK1 and MDCK-II cell lines was moderate-to-high for compound **7** and low for compound **8** (Table 5).

Table 5. In vitro solubility and permeability of compounds **7** and **8**.

Compound	Solubility (FaSSiF)[a]	Solubility (SGF)[b]	Permeability (cm^{-6}/sec)	
			LLC-PK1	MDCK-II
7	0.058 mg/mL	0.03 mg/mL	14.8	22.9
8	0.03 mg/mL	0.017 mg/mL	6.7	8.4

[a] FaSSiF at pH= 6.5, t= RT, time= 4 h. [b] SGF pH= 1.8, t= RT, time= 4 h.

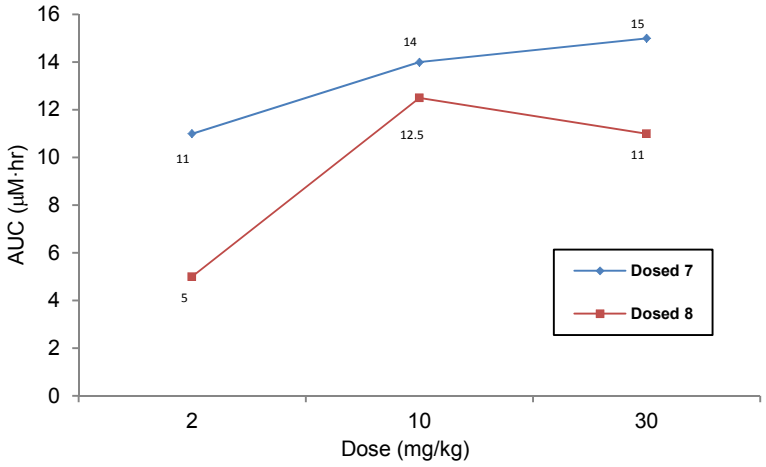

Figure 5. Oral dose escalation studies in dog with compound **7** and **8.**

Considering the exceptional virological and PK profiles of **7** and **8**, we were now challenged to address the major constraint of insufficient oral exposure in our preclinical species. As such, our goal turned to the identification of prodrugs of **7** and **8** that would achieve the highest possible plasma exposures of the parent compound to enable long-term oral non-rodent safety studies, and subsequently enable IND human studies. A thorough inspection of the scientific literature[22,23] led us to consider several opportunities to address the identified physicochemical limitations.

The molecular structure of compounds **7** and **8** provided two distinct hydroxyl functional groups for the introduction of permeability and/or solubility enhancing pro-moieties (a and b, Figure 6). By employing in silico tools,[24] we were able to systematically design prodrugs to independently evaluate the impact of an increase in solubility and then permeability. As part of the discovery efforts, we evaluated established promoeities known to enhance plasma exposure via mechanisms involving active transport, colonic absorption, circulating prodrugs, and lipidic prodrug uptake.

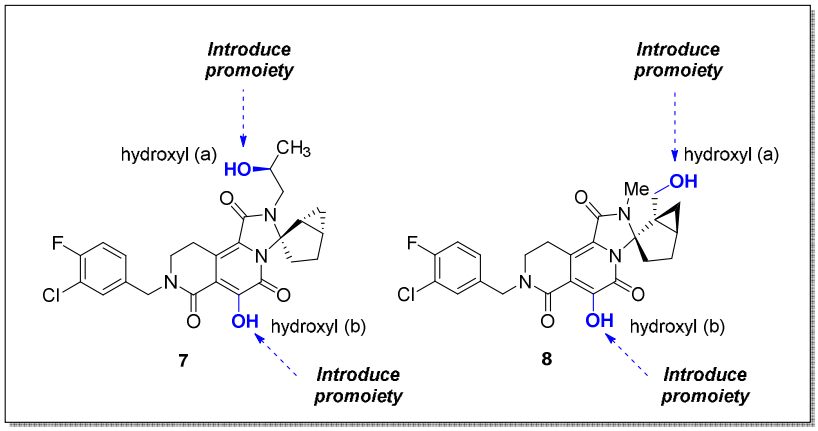

Figure 6. Hydroxyl groups (a and b) for introduction of pro-moieties.

Our initial prodrug strategy sought to address the limited aqueous (FaSSiF/SGF) solubilities of our lead molecules. To this end, we selected parent compound **7** for further interrogation. We focused our efforts on the installation of solubility-enhancing phosphate and aminoester promoieties at both positions, but found challenges with chemical stability and synthesis with such groups installed at the aromatic hydroxyl (b) of the core. However, numerous prodrugs at the aliphatic hydroxyl position (a) were successfully prepared and characterized, and two distinct leads emerged, **P1**-7 and **P2-7**, which are highlighted in Table 6. Importantly, both prodrugs

provided the intended marked improvements in FaSSiF solubility to >2 mg/mL. **P1-7** exhibited the anticipated loss in cell-based potency due to the inefficient permeability imparted by the ionizable phosphate group, while **P2-7** maintained its potency due to either efficient uptake of the prodrug or extracellular esterase-mediated bioconversion to parent.

Table 6. Profiles of solubility-enhancing prodrugs **P1-7** and **P2-7**.

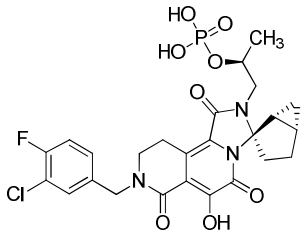

P1-7

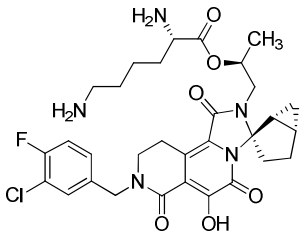

P2-7

Compound	WT IP[a]	Solubility (FaSSiF)[b]	Stability at 37 °C (FaSSiF, SGF)
P1-7	1580 nM	2.3 mg/mL	>98% for 4 h
P2-7	40 nM	>2 mg/mL	90% for 4 h

[a] kinetic HIV replication assay IP in 0% NHS.[16] [b] FaSSiF at pH= 6.5, t= RT, time= 4 h.

We identified efficient means by which to prepare these classes of prodrugs directly and selectively from their parent compound **7** (Scheme 7). **P1-7** was synthesized in high yield by treatment of **7** with diphosphoryl chloride at low temperature followed by an *in situ* basic hydrolysis to the desired phosphate. Correspondingly, **P2-7** was prepared by selective esterification of the secondary hydroxyl group followed by Boc-deprotection to afford the aminoester prodrug in high yield.

Scheme 7. Synthesis of **P1-7** and **P2-7**.

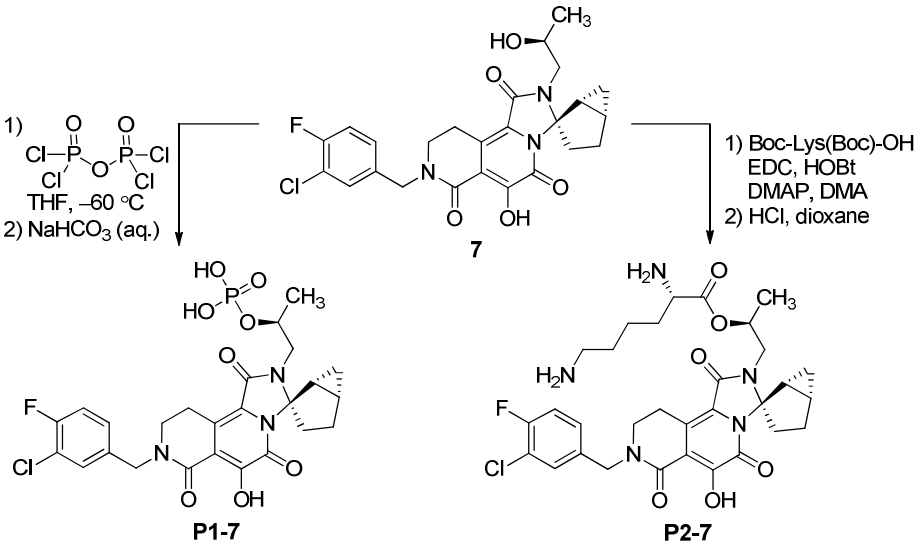

The PK profiles of **P1-7** and **P2-7** in dog were evaluated and are summarized in Figure 7. Over the time-course of these studies, circulating levels of both prodrug and parent were measured, and due to the known plasma instability of both compounds, collected blood samples were immediately stabilized with dichlorovos.[25] When dosed iv, **P1-7** and **P2-7** displayed expected high clearance with no significant detectable levels of circulating prodrug. At a low oral dose of 2 mg/kg, both compounds provided good exposures of parent (AUC= 6.8–9.6 μM•hr), consistent with those observed from a direct oral dose of **7**. Unfortunately, dose escalation revealed that the previously observed exposure plateau was not sufficiently remedied through this prodrug strategy. Oral dose ranging studies up to 300 mg/kg provided relatively little improvement in AUC, with this highest dose providing a maximum 6-fold improvement in exposure over the 2 mg/kg dose. As a result, efforts toward solubility-enhancing prodrugs were suspended. These exposure data suggested that parent solubility was not the only factor limiting

compound absorption, and rather indicated that limited parent permeability may be an additional culprit.

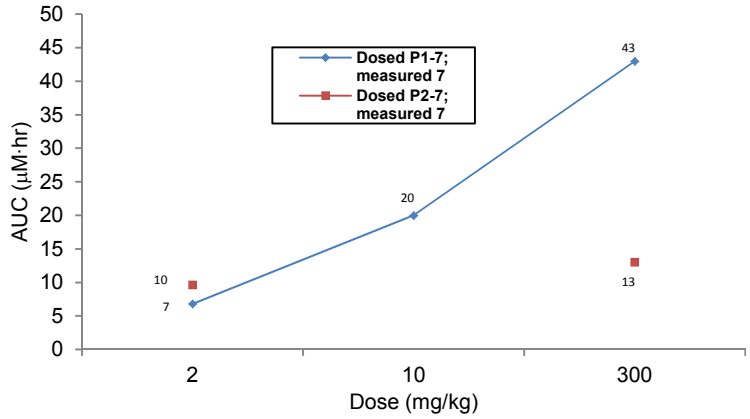

Figure 7. Oral dose escalation studies in dog with compound **P1-7** and **P2-7** measuring exposures of **7**. The indicated doses have been normalized to account for the promiety of each prodrug, and represent the actual dose of parent administered.

We next turned our focus towards the phenolic hydroxyl group (b) of the requisite bidentate metal binding pharmacophore inherent to all HIV InSTis, including compounds **7** and **8**. Based on our previous experience with prodrugs of RAL,[26,27] we suspected that the acidity and the ionizability of this hydroxyl group was likely impacting the permeability of the parent compounds. Therefore we devised a similar strategy utilizing the acetal carbonate functionality as a permeability-enhancing pro-moiety. The acetal carbonate group provided two distinct points of chemical diversity that could be used to modulate physicochemical properties. Indeed, using in silico methods, the isopropyl acetal carbonate was identified to provide the greatest predicted increase in permeability with minimal negative impact on solubility, and was therefore initially prioritized for synthesis on both parent compounds.

Chemical synthesis of the acetal carbonate prodrugs was initiated from parent molecules **7** and **8** using commercially available haloalkyl carbonates or haloalkyl carbonates synthesized using established procedures.[28] From parent **7**, alkylation by the in situ-generated corresponding alkyl iodide of chloromethyl isopropyl carbonate provided prodrug **P3-7** in good yield (Scheme 8). Prodrug **P3-8** was synthesized using a similar procedure starting with parent **8** and iodomethyl isopropyl carbonate which provided improved chemical yields (Scheme 9). Synthesis of both prodrugs was robust and provided multi-gram quantities for high-dose PK studies.

Scheme 8. Synthesis of **P3-7**.

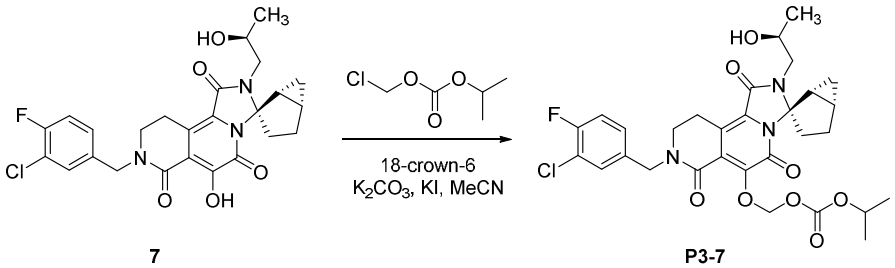

7

cLogP = 2.15

Predicted P_{app} = 9 cm^{-6}/sec

P3-7

cLogP = 3.12

Predicted P_{app} = 28 cm^{-6}/sec

Scheme 9. Synthesis of **P3-8**.

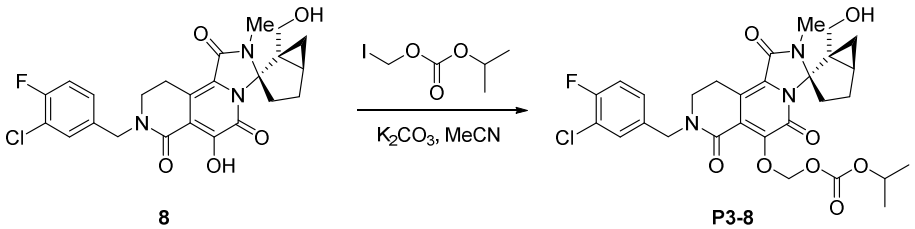

8

cLogP = 0.8

Predicted P_{app} = 13 cm^{-6}/sec

P3-8

cLogP = 1.4

Predicted P_{app} = 28 cm^{-6}/sec

P3-7 and **P3-8** displayed excellent SGF stability up to 4 hours and provided an increase in FaSSiF and SGF solubility over their parent compounds (Table 7). As expected based on literature precedent, the acetal carbonate promoieties underwent rapid esterase-mediated bioconversion in plasma, and exhibited overall improved in vitro permeability compared to the parent compounds. Both prodrugs **P3-7** and **P3-8** met the in vitro selection criteria and were evaluated in rising oral dose PK studies in dog.

Table 7. In vitro profiles of permeability-enhancing prodrugs **P3-7** and **P3-8**.

Compound	WT IP[a]	Solubility (FaSSiF)[b]	Stability at 37 °C (FaSSiF, SGF)	Permeability (cm^{-6}/sec)	
				LLC-PK1	MDCK-II
P3-7	178 nM	0.25 mg/mL	>98% for 4 h	26.7	23.5
P3-8	16 nM	0.50 mg/mL	>98% for 4 h	26.5	19.7

[a] kinetic HIV replication assay IP in 0% NHS.[16] [b] FaSSiF at pH= 6.5, t= RT, time= 4 h.

At an initial 2 mg/kg dose of **P3-7**, a 2-fold increase in exposure of **7** was observed compared to exposure from an equivalent 2 mg/kg dose of **7** (23 μM•hr vs. 11 μM•hr) (Figure 8). We were gratified to observe a dose-proportional increase in exposure of **7** to 128 μM•hr after a 5-fold increase in the **P3-7** dose (2 mg/kg to 10 mg/kg). However, a plateau in exposure of **7** manifested after a further 3-fold dose increase of **P3-7** (10 mg/kg to 30 mg/kg). We suspected that the insufficient solubility of **P3-7** likely contributed to the early exposure plateau and therefore initiated efforts towards addressing this limitation (*vide infra*).

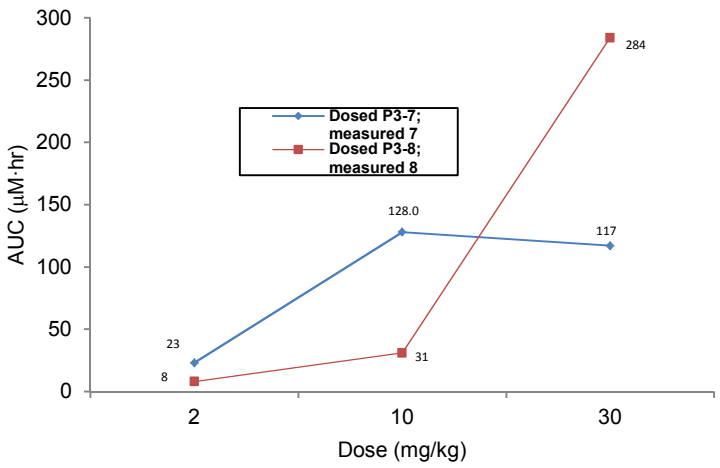

Figure 8. Oral dose escalation studies in dog with prodrugs **P3-7** and **P3-8** measuring exposures of **7** and **8**. The indicated doses have been normalized to account for the promoiety of each prodrug, and represent the actual dose of parent administered.

In contrast to **P3-7**, an initial 2 mg/kg dose with **P3-8** did not provide a similar increase in exposure of **8** compared to exposure from an equivalent 2 mg/kg dose of **8** (5 μM•hr vs. 8 μM•hr). After the standard 5-fold increase in dose of **P3-8** (2 mg/kg to 10 mg/kg), a near 4-fold increase in exposure of **8** was observed. Interestingly, at the next 3-fold increase in dose of **P3-8** (10 mg/kg to 30 mg/kg), exposures of **8** reached 284 μM•hr, which was considered to provide sufficient in vivo exposure of **8** to enable toxicology studies.

To study the relative contribution of hepatic versus extrahepatic conversion of **P3-7** and **P3-8** to their respective parent molecules, **P3-7** and **P3-8** were dosed to portal vein-cannulated dogs and the concentrations of prodrugs and parent molecules were determined in plasma collected from the portal and jugular veins (Tables 8 and 9). Following oral administration of both prodrugs at doses corresponding to 10 mg/kg of the respective parent molecules, low levels of **P3-7** and **P3-8** were measured in the portal vein along with high plasma levels of the respective

parents, suggesting most of the prodrug converts rapidly to parent before reaching the liver. The prodrug levels diminished quickly in systemic circulation, highlighting efficient in vivo conversion to both parent molecules.

Table 8. Profiles of prodrug **P3-7** in portal vein-cannulated dogs.

10 mg/kg p.o. dose **P3-7**[a]	AUC (μM·hr)		Percent (%) **P3-7** measured
	P3-7	**7**	
Portal vein	1.12	23.9	5%
Jugular vein	0.034	33.9	0.1%

[a] The indicated dose has been normalized to account for the promoiety, and represents the actual dose of **7** administered.

Table 9. Profiles of prodrug **P3-8** in portal vein-cannulated dogs.

10 mg/kg p.o. dose **P3-8**[a]	AUC (μM·hr)		Percent (%) **P3-8** measured
	P3-8	**8**	
Portal vein	2.55	27.3	9%
Jugular vein	0.037	30.4	0.1%

[a] The indicated dose has been normalized to account for the promoiety, and represents the actual dose of **8** administered.

Oral administration of the carbonate acetal prodrug **P3-7** provided significant improvements in high-dose parent exposure over direct administration of **7**. However, we remained interested in further exploring the limitations of our prodrug strategy. While we identified and addressed parent compound permeability as a primary contributing factor to the poor high-dose exposures of **7**, the observed exposure plateau of **P3-7** (10 to 30 mg/kg doses) suggested to us that

compromised compound solubility remained a contributing liability (*vide supra*). Therefore, we sought to combine two promoieties targeting both solubility and permeability into a single compound through a "double" prodrug approach to provide additional exposure enhancements. To this end, we synthesized prodrug **P4-7** bearing a phosphate group on the aliphatic hydroxyl (a) and a carbonate acetal on the aromatic hydroxyl (b).

As expected, **P4-7** maintained a profile similar to the previously described prodrug **P1-7**, with poor cell-based potency, excellent solubility, good FaSSiF and SGF stability, and poor plasma stability (Table 10). Upon oral dose escalation of **P4-7** in the dog, we were gratified to achieve high and dose proportional exposures of parent 7 up to 100 mg/kg (Figure 9). At this highest dose tested, we were able to attain a parent plasma exposure of 570 μM•hr, the highest oral exposure achieved to date from this compound class. This significantly exceeded our initial exposure target, and provided a path by which to also move **7** into toxicology studies and support compound advancement.

Table 10. Profile of "double" prodrug **P4-7**.

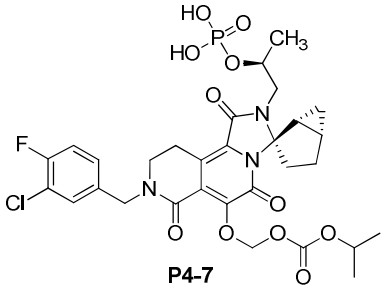

P4-7

Compound	WT IP[a]	Solubility (FaSSiF)[b][	Stability at 37 °C (FaSSiF, SGF)
P4-7	>4200 nM	>2 mg/mL	>98% for 4 h

[a] kinetic HIV replication assay IP in 0% NHS.[16] [b] FaSSiF at pH= 6.5, t= RT, time= 4 h.

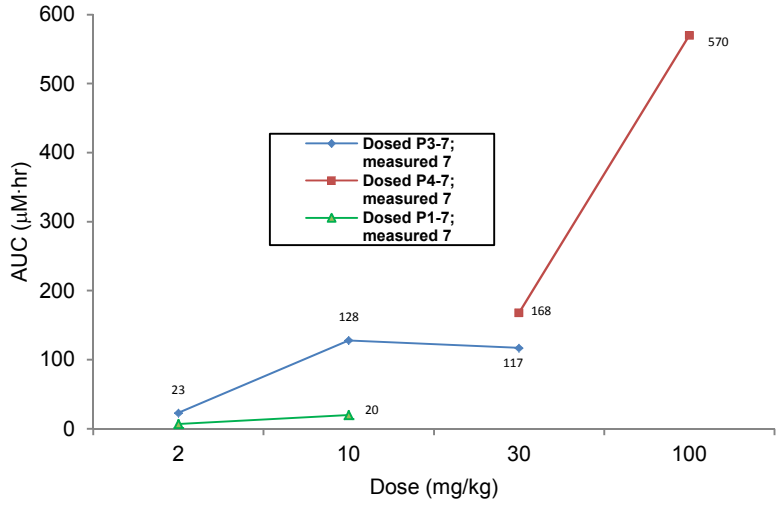

Figure 9. Comparison of oral dose escalation studies in dog with **P1-7**, **P3-7** and **P4-7** measuring exposures of parent **7**. The indicated doses have been normalized to account for the promoiety of each prodrug, and represent the actual dose of parent administered.

CONCLUSION

We have described the discovery of two next-generation HIV integrase strand transfer inhibitors, **7** and **8**, based on the 2-pyridinone core of MK-0536. Both compounds exhibit excellent WT potency, a flat mutation profile, and preclinical PK projecting a once-daily human dose. In advancing both compounds toward non-rodent safety and tolerabilty studies, we learned that **7** and **8** suffered from less than dose proportional oral exposure, with plasma concentrations plateauing below a 10 mg/kg dose. These exposures were attributed to compromised absorption due to poor physicochemical properties, and a prodrug strategy was undertaken to address these issues by targeting compounds to independently enhance both parent solubility and parent permeability. While solubility-enhancing prodrugs on their own did not sufficiently address

limitations of either parent compound, we were able to achieve high parent plasma exposures by masking the acidic phenol of the InSTi pharmacophore with a carbonate acetal promoiety. Carbonate acetal prodrug **P3-8** provided high oral exposures of parent 8, while "double" prodrug **P4-7** (carbonate acetal, phosphate), was required to achieve similar high exposures of **7**. Our innovative prodrug strategy successfully addressed key limitations of **7** and **8**, and provided a path by which to further advance both compounds.

EXPERIMENTAL SECTION

All experimental procedures, characterization data for new compounds, in vitro and in vivo experimental protocols, and details on computational modeling and X-ray crystallographic data are available in the Supporting Information section free of charge via the Internet at http://pubs.acs.org.

Compound purity and identity for intermediates were determined by LC-MS and/or ^{1}HNMR. Compound purity and identity for final compounds were determined by LC-MS and ^{1}HNMR. In all cases, final compounds possess purity ≥95%.

ASSOCIATED CONTENT

Supporting Information. All Supporting Information is available free of charge on the ACS Publications website at http://pubs.acs.org.

PDB ID Codes. Coordinates and structure factors for PFV Integrase with compounds **7** and **8** have been deposited in the Protein Data Bank[29] with accession numbers 4ZTF and 4ZTJ, respectively.

AUTHOR INFORMATION

Corresponding Author

*E-mail: izzat_raheem@merck.com. Phone: (215) 652-2734. Fax: (215) 652-7310.

*E-mail: abbas_walji@merck.com. Phone: (215) 652-3379. Fax: (215) 652-7310.

Author Contributions

‡ I.T.R and A.W. contributed equally.

ACKNOWLEDGMENTS

The authors thank the Merck West Point NMR and Mass Spectrometry facilities for assistance in characterizing the compounds presented in this manuscript. The authors also gratefully acknowledge Dr. Deanne Rudd and Kenneth Anderson for identifying ex vivo prodrug stabilization conditions to support prodrug bioanalysis. We are grateful to the scientists at WuXi-AppTec for their assistance in synthesizing valuable intermediates and final compounds.

ABBREVIATIONS USED

AUC, area under the plasma concentration-time curve; CL_{int}, intrinsic clearance; CL_p, plasma clearance; CL_u, unbound plasma clearance; CYP, cytochrome P450; DABCO, 1,4-diazabicyclo[2.2.2]octane; DIPEA, diisopropyl ethylamine; DMA, dimethylacetamide; DMF,

dimethylformamide; DNA, deoxyribonucleic acid; DTG, Dolutegravir; EDC, 1-ethyl-3-(3-dimethylaminopropyl)carbodiimide; ELV, Elvitegravir; EtOH, ethanol; F, bioavailability; FaSSiF, fasted simulated intestinal fluid; H-bond, hydrogen bond; HIV, human immunodeficiency virus; InSTI, integrase strand transfer inhibitor; IP, inflection point; iv, intravenous; Me, methyl; MeCN, acetonitrile; MeOH, methanol; MTBE, methyl *tert*-butylehter; NHS, normal human serum; nM, nanomolar; NMO, *N*-methylmorpholine *N*-oxide; PFV, prototype foamy virus; PivCl, pivaloyl chloride; PK, pharmacokinetic; p.o., oral; PSA, polar surface area; RAL, Raltegravir; RT, room temperature; SGF, simulated gastric fluid; THF, tetrahydrofuran; TMSOTf, trimethylsilyl trifluoromethanesulfonate; TPAP, tetrapropylammonium perruthenate; WT, wild-type.

REFERENCES

(1) Rowley, M. The Discovery of Raltegravir, an Integrase Inhibitor for the Treatment of HIV Infection. *Prog. Med. Chem.* **2008***, 46*, 1−28.

(2) Evering, T. H.; Markowitz, M. Raltegravir (MK-0518): An Integrase Inhibitor for the Treatment of HIV-1. *Drugs Today* **2007***, 43*, 865−877.

(3) Dayam, R. G. R.; Al-Mawsawi, L. Q.; Neamati, N. HIV-1 Integrase Inhibitors: 2005-2006 Update. *Med. Res. Rev.* **2008***, 28*, 118−154.

(4) Karmon, S. L.; Markowitz, M. Next-generation Integrase Inhibitors: Where to After Raltegravir? *Drugs* **2013***, 73*, 213−228.

(5) Croxtall, J. D.; Scott, L. J. Raltegravir: In Treatment-naive Patients with HIV-1 Infection. *Drugs* **2010**, *70*, 631−642.

(6) Métifiot, M.; Marchand, C.; Pommier, Y. HIV Integrase Inhibitors: 20-year Landmark and Challenges. *Advances in Pharmacology* **2013**, *67*, 75−105.

(7) Di Santo, R. Inhibiting the HIV Integration Process: Past, Present, and the Future. *J. Med. Chem.* **2014**, *57*, 539−566.

(8) Klibanov, O. M. Elvitegravir, an Oral HIV Integrase Inhibitor, for the Potential Treatment of HIV Infection. *Curr. Opin. Investig. Drugs* **2009**, *10*, 190−200.

(9) Reviriego, C. Elvitegravir for the Treatment of HIV Infection. *Drugs of Today* **2014**, *50*, 209−217.

(10) Katlama, C.; Murphy, R. Dolutegravir for the Treatment of HIV. *Expert Opin. Investig. Drugs.* **2012**, *21*, 523−530.

(11) Bar–Magen, T.; Sloan, R. D.; Donahue, D. A.; Kuhl, B. D.; Zabeida, A.; Xu., H.; Oliveira, M.; Hazuda, D. J.; Wainberg, M. A. Identification of Novel Mutations Responsible for Resistance to MK-2048, a Second-generation HIV-1 Integrase Inhibitor. *J. Virol.* **2010**, *84*, 9210−9216.

(12) (a) Wiscount, C. M.; Williams, P. D.; Tran, L. O.; Embrey, M. W.; Fisher, T. E.; Sherman, V.; Homnick, C. F.; Staas, D. D.; Lyle, T. A.; Wai, J. S.; Vacca, J. P.; Wang, Z.; Felock, P. J.; Stillmock, K. A.; Witmer, M. V.; Miller, M. D.; Hazuda, D. J.; Day, A. M.; Gabryelski, L. J.; Ecto, L. T.; Schleif, W. A.; DiStefano, D. J.; Kochansky, C. J.; Anari, M. R. 10-Hydroxy-7,8-dihydropyrazino[1',2':1,5]pyrrolo[2,3-d]pyridazine-1,9(2H,6H)-diones: Potent,

Orally Bioavailable HIV-1 Integrase Strand-transfer Inhibitors with Activity Against Integrase Mutants. *Bioorg. Med. Chem. Lett.* **2008***, 18,* 4581−4583. (b) Quashie, P.K., Sloan, R.D., Wainberg, M.A. Novel Therapeutic Strategies Targeting HIV Integrase. *BMC Med,* **2012**, *10*, 34. (c) Vacca, J.; Fisher, T.; Embrey, M.; Hazuda, D.; Miller, M.; Felock, P.; Witmer, M.; Gabryelski, L. J.; Lyle, T.A. Discovery of MK-2048: Subtle Changes Confer Unique Resistance Properties to a Series of Tricyclic Hydroxypyrrole Integrase Strand Transfer Inhibitors. Presented at the 4th IAS Conference, Sydney, Australia, **2007**. Talk WEPEA088. (d) Wai J., Fisher T., Embrey, M.; Egbertson, M.; Vacca, J.; Hazuda, D.; Miller, M.; Witmer, M.; Gabryelski, L.; Lyle, T. Next Generation of Inhibitors of HIV-1 Integrase Strand Transfer Inhibitor: Structural Diversity and Resistance Profiles. Presented at the CROI, Los Angeles, CA, **2007**. Talk #87.

(13) Métifiot, M.; Johnson, B.; Smith, S.; Zhao, X. Z.; Marchand, C.; Burke, T.; Hughes, S.; Pommier, Y. MK-0536 Inhibits HIV-1 Integrases Resistant to Raltegravir. *Antimicrob. Agents Chemother.* **2011***, 55*, 5127−5133.

(14) Egbertson, M. S.; Wai, J. S.; Cameron, M.; Hoerrner, R. S. Discovery of MK-0536: A Potential Second-Generation HIV-1 Integrase Strand Transfer Inhibitor with a High Genetic Barrier to Mutation. In *Antiviral Drugs: From Basic Discovery through Clinical Trials*; Kazmierski, W.M., Ed.; John Wiley & Sons, Inc., **2011**; pp 163–180.

(15) Tang, H.; Hussain, A.; Leal, M.; Mayersohn, M.; Fluhler, E. *Drug Metabolism and Disposition* **2007**, *35*, 1886−1893.

(16) For details see Supporting Information.

(17) (a) Hare, S.; Vos, A. M.; Clayton, R. F.; Thuring, J. W.; Cummings, M. D.; Cherepanov, P. Molecular Mechanisms of Retroviral Integrase Inhibition and the Evolution of Viral Resistance. *Proc. Natl. Acad. Sci.* USA. **2010**, *107*, 20057−20062. (b) Hare, S.; Gupta, S. S.; Valkov, E.; Engelman, A.; Cherepanov, P. Retroviral Intasome Assembly and Inhibition of DNA Strand Transfer. *Nature* **2010**, *464*, 232−236.

(18) (a) Hare, S; Smith, S. J.; Métifiot, M.; Jaxa-Chamiec, A.; Pommier, Y.; Hughes, S. H.; Cherepanov, P. Structural and Functional Analyses of the Second-generation Integrase Strand Transfer Inhibitor Dolutegravir (S/GSK1349572). *Mol. Pharmacol*. **2011**, *80*, 565−572. (b) Métifiot, M.; Maddali, K.; Johnson, B. C.; Hare, S.; Smith, S. J.; Zhao, X. Z.; Marchand, C.; Burke, T. R.; Hughes, S. H.; Cherepanov, P.; Pommier, Y. Activities, Crystal Structures, and Molecular Dynamics of Dihydro-1H-isoindole Derivatives, Inhibitors of HIV-1 Integrase. *ACS Chem. Biol*. **2013***, 8*, 209−217. (c) Desimmie, B. A.; Demeulemeester, J.; Suchaud, V.; Taltynov, O.; Billamboz, M.; Lion, C.; Bailly, F.; Strelkov, S. V.; Debyser, Z.; Cotelle, P.; Christ, F. 2-Hydroxyisoquinoline-1,3(2H,4H)-diones (HIDs), Novel Inhibitors of HIV Integrase with a High Barrier to Resistance. *ACS Chem. Biol.* **2013**, *8*, 1187−1194.

(19) SZYBKI, version 1.8.0.1, OpenEye Scientific Software, Inc., Santa Fe, NM, USA, www.eyesopen.com, **2013**.

(20) Alorati, A.D.; Bio, M.M.; Brands, K.M.J; Cleator, E.; Davies, A.J.; Wilson, R.D.; Wise, C.S. A Practical and Scaleable Synthesis of 1R,5S-Bicyclo[3.1.0]hexan-2-one: The Development of a Catalytic Lithium 2,2,6,6-Tetramethylpiperidide (LTMP) Mediated Intramolecular Cyclopropanation of (R)-1,2-Epoxyhex-5-ene. *Org. Proc. Res. Dev.* **2007**, *11*, 637−641.

(21) Takeda, H.; Honma, M.; Ida, R.; Sawada, T.; Nakada, M. Catalytic Asymmetric Intramolecular Cyclopropanation of 2-diazo-6-heptenoic Acid Esters. *Synlett.* **2007**, *4*, 579−582.

(22) Stella, V. J.; Borchardt, R. T.; Hageman, M. J.; Oliyai, R.; Maag, H. Tilley, J. *Prodrugs: Challenges and Rewards Part 1 and Part 2*; Springer: New York, **2007**.

(23) Rautio, J.; Kumpulainen, H.; Heimbach, T.; Oliyai, R.; Oh, D.; Järvinen, T.; Savolainen, J. Prodrugs: Design and Clinical Applications. *Nat. Rev. Drug Discov.* **2008***, 7*, 255−270.

(24) (a) The octanol/water partition coefficient (ALogP98) was calculated using Accelrys Cerius2 Software (Accelrys, Inc., San Diego, CA, USA). (b) Clark, D. E. *J. Pharm. Sci.* **1999**, *88*, 807−814. (c) Sherer, E.C; Verras, A.; Madeira, M.; Hagmann, W. K.; Sheridan, R. P.; Roberts, D.; Bleasby, K.; Cornell, W. *Molecular Informatics*. **2012**, *31*, 231−245.

(25) Fung, E.N.; Zheng, N.; Arnold, M.E.; Zeng, J. Effective Screening Approach to Select Esterase Inhibitors used for Stabilizing Ester-containing Prodrugs Analyzed by LC-MS/MS. *Bioanalysis* **2010**, *2*, 733−743.

(26) Walji, A.M.; Sanchez, R.I.; Clas, S.D.; Nofsinger, R.; de Lera Ruiz, M; Li, J.; Bennet, A.; John, C.; Bennett, D.J.; Sanders, J.M.; Di Marco, C.N.; Kim, S.H.; Balsells, J.; Ceglia, S.S.; Dang, Q.; Manser, K.; Nissley, B.; Wai, J.S.; Hafey, M.; Wang, J.; Chessen, G.; Templeton, A.; Higgins, J.; Smith, R.; Wu, Y.; Grobler, J.; Coleman, P.J. Discovery of MK-8970: An Acetal Carbonate Prodrug of Raltegravir with Enhanced Colonic Absorption. *Chem Med Chem* **2015**, *10*, 245−252.

(27) Nofsinger, R.; Clas, S.-D.; Sanchez, R. I.; Walji, A. M.; Manser, K.; Nissley, B.; Balsells, J.; Nair, A.; Dang, Q.; Bennett, D. J.; Hafey, M.; Wang, J.; Higgins, J.; Templeton, A.; Coleman,

P.; Grobler, J.; Smith, R.; Wu, Y. Design of Prodrugs to Enhance Colonic Absorption by Increasing Lipophilicity and Blocking Ionization. *Pharmaceuticals* **2014**, *7*, 207−219.

(28) Thomas, J. D.; Sloan, K. B. Overcoming Steric Effects in the Coupling Reaction of Alkoxycarbonyloxymethyl (AOCOM) Halides with Phenols: An Efficient Synthesis of AOCOM Phenolic Prodrugs. *Tetrahedron Lett.* **2007**, *48*, 109−112.

(29) Berman, H. M.; Westbrook, J.; Feng, Z.; Gilliand, G.; Bhat, T. N.; Weissig, H.; Shindyalov, I. N.; Bourne, P. E. The Protein Data Bank. *Nucleic Acids Res.* **2000**, *28*, 235−242.

TABLE OF CONTENTS GRAPHIC